

Phase Structure of the Random-Plaquette Z_2 Gauge Model: Accuracy Threshold for a Toric Quantum Memory

Takuya Ohno¹

Department of Electrical and Computer Engineering, Graduate School of Engineering, Nagoya
Institute of Technology, Nagoya 466-8555 Japan

Gaku Arakawa²

Department of Applied Physics, Graduate School of Engineering, Nagoya Institute of Technology,
Nagoya 466-8555 Japan

Ikuo Ichinose³

Department of Applied Physics, Graduate School of Engineering, Nagoya Institute of Technology,
Nagoya, 466-8555 Japan

Tetsuo Matsui⁴

Department of Physics, Kinki University, Higashi-Osaka, 577-8502 Japan

Abstract

We study the phase structure of the random-plaquette Z_2 lattice gauge model in three dimensions. In this model, the “gauge coupling” for each plaquette is a quenched random variable that takes the value β with the probability $1 - p$ and $-\beta$ with the probability p . This model is relevant for the recently proposed quantum memory of toric code. The parameter p is the concentration of the plaquettes with “wrong-sign” couplings $-\beta$, and interpreted as the error probability per qubit in quantum code. In the gauge system with $p = 0$, i.e., with the uniform gauge couplings β , it is known that there exists a second-order phase transition at a certain critical “temperature”, $T(\equiv \beta^{-1}) = T_c = 1.31$, which separates an ordered(Higgs) phase at $T < T_c$ and a disordered(confinement) phase at $T > T_c$. As p increases, the critical temperature $T_c(p)$ decreases. In the p - T plane, the curve $T_c(p)$ intersects with the Nishimori line $T_N(p)$ at the certain point $(p_c, T_N(p_c))$. The value p_c is just the accuracy threshold for a fault-tolerant quantum memory and associated quantum computations. By the Monte-Carlo simulations, we calculate the specific heat and the expectation values of the Wilson loop to obtain the phase-transition line $T_c(p)$ numerically. The accuracy threshold is estimated as $p_c \simeq 0.033$.

¹e-mail address: taquya@phys.kyy.nitech.ac.jp

²e-mail address: e101608@phys.kyy.nitech.ac.jp

³e-mail address: ikuo@nitech.ac.jp

⁴e-mail address: matsui@phys.kindai.ac.jp

1 Introduction

Gauge theory plays a very important role in modern physics. All the interactions between elementary particles are described by gauge theories. Furthermore, gauge theories present important and clear understandings for other areas of physics including superconductivity, fractional quantum Hall effect, random spin systems, localization by random vector potentials.

Recent developments of nanotechnology elevate the old interesting theoretical ideas to realistic objects. Quantum computer(QC) is one of them. One of the most difficult problem for constructing QC is how to keep quantum states stable against noises while quantum computations are performed, i.e., the problem of decoherence. In order to make a quantum computation fault-tolerant, the involved quantum states should have certain “quantum numbers”, and these quantum numbers are required to stay as good ones during the computation. From this point of view, one may expect that gauge-theory mechanisms like Aharonov-Bohm(AB) effect play an important role in quantum computation.

In fact, Kitaev[1] recently proposed a fault-tolerant quantum memory and quantum computations that are based on the AB effect of discrete Z_2 gauge symmetry. After that many interesting studies on Kitaev’s model appeared[2, 3, 4, 5, 6, 7, 8]. Among them, two of the present authors[7] generalized Kitaev’s model and also clarified the relationship between Kitaev’s model and a *spontaneously broken* $U(1)$ gauge theory.

For quantum computations, it is important to estimate its accuracy threshold. As discussed in Ref.[4], it is obtained for Kitaev’s model by studying the random-plaquette gauge model(RPGM) on a three-dimensional ($3D$) lattice with Z_2 gauge symmetry. In the RPGM, the (inverse) gauge coupling for each plaquette takes the values $\pm\beta$ with random sign; the probability to take β is given by $1 - p$ and the probability of “wrong-sign” $-\beta$ is p . The original nonrandom ($p = 0$) $3D$ Z_2 lattice gauge theory is known to be dual to the classical $3D$ Ising model. The fluctuations of gauge field are controlled by the “temperature” (the coupling constant) $T \equiv \beta^{-1}$. The system exhibits a second-order phase transition at the critical temperature $T = T_c = 1.31$. For $T < T_c$ the gauge-field fluctuations are small and the system is in the ordered Higgs phase, while for $T_c < T$, the fluctuations are large and the system is in the disordered confinement phase[9]. As p increases from $p = 0$, the critical temperature $T_c(p)$ decreases due to the randomness in gauge couplings, and it shall vanish at a certain value p_0 , $T_c(p_0) = 0$. In Fig.1, we illustrate a schematic phase diagram in the $p - T$ plane. The solid line expresses $T_c(p)$, which may decrease very rapidly near p_0 . The dashed line is the Nishimori line $T(p) = T_N(p)$ [10] on which fluctuations of gauge field caused by the quantum effect and those caused by the random couplings are equal. As we explain it in detail later

on, we consider a particular method of error corrections in QC's that is realized along the Nishimori line. Also the system should be in the ordered Higgs phase in order that the quantum computations are fault-tolerant. Thus the intersection point of the critical line $T_c(p)$ and the Nishimori line, i.e., $T_c(p_c) = T_N(p_c)$, locates the accuracy threshold for the quantum computations by Kitaev's model. One concludes that the quantum computations are fault-tolerant for $p < p_c$.

The present paper is organized as follows. In Sec.2, we shall review Kitaev's model of a quantum toric code and its relation to the Z_2 gauge model. In Sec.3, the relationship between the accuracy threshold of the toric code and the random spin and gauge models is discussed. Section 4 is the main part of the present paper. We present the results of Monte-Carlo simulations of the RPGM. We calculate the specific heat and expectation values of the Wilson loop for various points in the $p - T$ plane. There are (at least) two phases in the model; one is the ordered Higgs phase and the other is the disordered confinement phase. From these studies, we estimate the accuracy threshold of the toric code as $p_c \simeq 0.033$. This value of threshold is consistent with the previous studies[4, 8]. In Ref.[4], the Z_2 RPGM in 3D was investigated by studying the lowest-energy configurations for various random gauge couplings, and then the critical concentration along the $T = 0$ axis was estimated as $p_0 = 0.029$. By using specific symmetry of the model on the Nishimori line, it is proved that the above value gives a lower bound for the accuracy threshold p_c [10]. On the other hand in Ref.[8], the *four-dimensional* RPGM was studied. The value of p at the intersection point of the phase boundary and the Nishimori line of this model gives an upper bound of p_c of the RPGM in 3D. By using the self duality of the model, it is obtained as 0.11, which is much larger than our result of p_c . Section 4 is devoted for conclusion.

2 Quantum toric code

The quantum toric code was first proposed by Kitaev[1], and many interesting studies on that idea appeared after that. It is more transparent to formulate Kitaev's model as a Z_2 lattice gauge theory[7]. The quantum toric code is viewed as a set of qubits put on links of a two-dimensional($2D$) square lattice with the periodic boundary condition (i.e., a torus). Each link of this lattice is denoted as (x, i) where x is the site index and $i = 1, 2$ is the spatial direction index. The qubit residing on the link (x, i) is described by a quantum Z_2 variable Z_{xi} and its conjugate variable X_{xi} . Z_{xi} is regarded as the Z_2 gauge field, and so X_{xi} plays the role of the electric field. They satisfy the commutation relations like

$$X_{xi}Z_{xi} = -Z_{xi}X_{xi}, \quad X_{xi}Z_{yj} = Z_{yj}X_{xi} \quad \text{for } (x, i) \neq (y, j). \quad (1)$$

In the matrix representation, $Z_{xi} = \sigma_{xi}^z$ and $X_{xi} = \sigma_{xi}^x$, where σ^x and σ^z are 2×2 Pauli spin matrices.

Let us consider the following generalized Hamiltonian,

$$\begin{aligned}
H_{\mathcal{T}} &= H_Z + H_Z^\psi + H_Z^\varphi, \\
H_Z &= -\lambda_1 \sum_{\text{link}} X_{xi} - \lambda_2 \sum_{\text{plaquette}} ZZZZ + \text{H.c.}, \\
H_Z^\psi &= -\gamma \sum_{\text{link}} \psi_{x+i}^\dagger Z_{xi} \psi_x + M \sum_{\text{site}} \psi_x^\dagger \psi_x + \text{H.c.}, \\
H_Z^\varphi &= -\gamma \sum_{\text{link}} \varphi_{x+i}^\dagger Z_{xi} \varphi_x + M \sum_{\text{site}} \varphi_x^\dagger \varphi_x + \text{H.c.}, \tag{2}
\end{aligned}$$

where λ_1 and λ_2 are coupling constants, and ψ_x and φ_x are ‘‘relativistic’’ fermions sitting on site x with the mass M and the hopping parameter γ . They satisfy the canonical anticommutation relations like

$$\{\psi_x, \psi_y^\dagger\} = \delta_{xy}, \quad \{\varphi_x, \varphi_y^\dagger\} = \delta_{xy}. \tag{3}$$

The above Hamiltonian (2) is invariant under Z_2 local gauge transformation. In fact, we have

$$\begin{aligned}
G_x &\equiv \left(\prod_{(y,i) \in x} X_{yi} \right) e^{-\pi i (\psi_x^\dagger \psi_x - \varphi_x^\dagger \varphi_x)}, \\
[G_x, H_{\mathcal{T}}] &= 0, \tag{4}
\end{aligned}$$

where $(y, i) \in x$ denotes 4 links emanating from site x , and the operator G_x is the generator of gauge transformations. Respecting the gauge invariance of $H_{\mathcal{T}}$, the physical states $|phys\rangle$ should be gauge invariant, i.e., satisfy the following physical-state condition,

$$G_x |phys\rangle = |phys\rangle. \tag{5}$$

The Hamiltonian of Kitaev’s model is obtained by setting $\lambda_1 = 0, \lambda_2 = 1, \gamma = 0$ and $M = 2$ [7], and then the quantum space of the gauge field and that of the fermions are coupled only through the gauge-invariance condition. In this case, it is easy to see that the ground states $|GS\rangle_K$ satisfy the following conditions,

$$\begin{aligned}
\psi_x^\dagger \psi_x |GS\rangle_K &= 0, \quad \varphi_x^\dagger \varphi_x |GS\rangle_K = 0, \\
A_x |GS\rangle_K &= |GS\rangle_K, \quad B_P |GS\rangle_K = |GS\rangle_K, \tag{6}
\end{aligned}$$

for all the sites x and plaquettes P , where the operators A_x and B_P are defined as follows,

$$A_x = \prod_{(y,i) \in x} X_{yi}, \quad \text{and} \quad B_P = \prod_{(y,i) \in P} Z_{yi}. \tag{7}$$

These operators are called *stabilizers* or *check operators*. From Eq.(4), A_x is the generator of a local gauge transformation of the Z_2 gauge field Z_{xi} , and B_P measures Z_2 -gauge flux penetrating the plaquette P , i.e., $B_P = 1$ for fluxless states and $B_P = -1$ for fluxful states. Eq.(6) means that $|GS\rangle_K$ involve no fermions (pure-gauge state), gauge-invariant, and fluxless.

As the system is defined on the torus, the ground states are not unique but 4-fold degenerate. They satisfy Eq.(6) and are distinguished by a pair of “nonlocal” quantum numbers $Z_a(a = 1, 2)$ defined as

$$Z_a = \prod_{C_Z^a} Z_{xi}, \quad (8)$$

where $C_Z^a(a = 1, 2)$ are two noncontractible closed loops on the original lattice (see Fig.2). The ground states have the quantum numbers $(Z_1, Z_2) = (1, 1), (1, -1), (-1, 1)$ and $(-1, -1)$. Quantum informations for the toric code are stored in the above 4-fold degenerate ground states which work as a *fault-tolerant qudit*. Instead of Z_a , we can consider a set of conjugate quantum numbers $X_a(a = 1, 2)$ given by

$$X_a = \prod_{\tilde{C}_X^a} X_{xi}, \quad (9)$$

where \tilde{C}_X^a are nontrivial closed loops on the *dual* lattice (see Fig.2) and X_{xi} 's in (9) reside on the links of the original lattice that are crossed by \tilde{C}_X^a . It is easily verified that Z_a and $X_a(a = 1, 2)$ satisfy the same commutation relations with the Pauli matrices. Then the ground states are characterized by the quantum numbers $(X_1, X_2) = (1, 1), (1, -1), (-1, 1)$ and $(-1, -1)$.

The gauge-theory aspect of Kitaev's model becomes clear when we consider excitations in the system. Excitations obviously break the local condition (6) at some specific sites and/or plaquettes. As the stabilizers satisfy the identities like

$$\prod_{\text{all sites}} A_x = 1, \quad \text{and} \quad \prod_{\text{all pl's}} B_P = 1, \quad (10)$$

these excitations should appear in pairs. A simple example is the fermion-pair state with two fermions at x and y ,

$$|F; C_{xy}\rangle = \psi_y^\dagger \left(\prod_{C_{xy}} Z \right) \varphi_x^\dagger |GS\rangle_K, \quad (11)$$

where C_{xy} is a certain path on the *original* lattice connecting x and y . Another example is the vortex-pair state with two vortices at *dual* sites x^* and y^* ,

$$|V; \tilde{C}_{x^*y^*}\rangle = \left(\prod_{\tilde{C}_{x^*y^*}} X \right) |GS\rangle_K, \quad (12)$$

where $\tilde{C}_{x^*y^*}$ is a certain path on the *dual* lattice connecting x^* and y^* , and X 's in (12) are on the links crossing $\tilde{C}_{x^*y^*}$ (see Fig.3). Wave function of the state containing the above fermionic and

vortex excitations acquires nontrivial phase factors when one of the excitations winds around the other. This is the AB effect of the Z_2 gauge theory.

As explained above, quantum informations are stored in a set of the 4-fold degenerate ground-states, $\mathcal{L} = \{|GS\rangle\}$. During a quantum computation, quantum states in quantum memory are to be damaged by noises which cause decoherence of the quantum states. As a result, excited states appear, i.e., errors occur. One can check whether errors have occurred by measuring the operators $\psi_x^\dagger \psi_x$, $\varphi_x^\dagger \varphi_x$, A_x , and B_P in the quantum states and judging whether the conditions (6) are satisfied or not. We can correct these errors by applying suitable operators on the quantum states. For example, the state with vortex-type excitations can be corrected by applying the operator $(\prod X)$, a product of X_{xi} along the path appeared in the excited state, owing to the identity $X_{xi}^2 = 1$. On the other hand, for the charge-type excitations, the operator $\psi_y(\prod Z)\varphi_x$ does the job. But we note that we can know only the locations of vortices and/or charges but not that of the error chain itself. Therefore we should consider specific methods of the error corrections. As a results there exists an accuracy threshold p_c , i.e., if the error probability per qubit and per unit computer time exceeds p_c , we cannot perform successful error corrections in practical manner. The threshold can be estimated by studying the random-bond Ising model(RBIM) in $2D$ and/or the RPGM in $3D$, as we discuss it in the following section.

3 Accuracy threshold and RPGM

It is interesting and important to estimate the accuracy threshold p_c of the toric quantum code. The value of p_c should be compared with those of other quantum memories and quantum gates which are estimated as 10^{-6} to $1/300$ [11]. In the most of the previous studies, concatenated quantum error correcting codes were considered instead of the surface codes in the present study.

As discussed in detail in Ref.[3, 4], p_c of the toric code can be obtained by studying the RBIM in $2D$ and/or the Z_2 RPGM in $3D$. We note that p_c depends on the practical methods of error corrections which one employs. In the method of Ref.[4] it is estimated as $p_c = 0.029$. Here we shall review the estimation of p_c by using the statistical-mechanical models in two steps. In the first step, we assume that every measurement of check operators done in order to check the quantum states is perfect, i.e., without any errors. Then the relevant model to calculate p_c is shown to be the $2D$ RBIM. In the second step, we take into account the possible errors in measuring check operators themselves. In this case, the relevant model becomes the $3D$ Z_2 RPGM. The latter model resembles the $2D$ RPGM of the toric code discussed in the previous section, but the dimensions of two models are different. The third dimension is introduced as the time direction along which we measure check

operators successively.

Let us start the first step. There are two types of errors; (i) phase errors associated with fermion-pair states of (11) and (ii) spin-flip errors associated with vortex-pair states of (12). Since these two types of errors can be discussed in the same manner, we focus here on the phase errors. A typical example of phase-error syndrome is given in Fig.4. The sites marked by filled circles denote error sites on which the check operator A_x has the eigenvalue (-1) , while $A_x = 1$ on the remaining sites. This implies that a chain of the phase errors have occurred. In Fig.5, we show one of the simplest case of two phase-error sites, where the error chain containing all error links is denoted by E . Therefore on the boundary sites of E , $A_x = -1$. In order to correct these errors, we have to connect the error sites by a certain chain which we call E' , and apply a phase operator $(\prod Z_{xi})$ along E' upon the quantum state under problem. There is of course ambiguity in choosing a suitable E' . Let us see this in detail. Because E plus E' form a closed loop, i.e., a cycle, the corrected state and the original state differ by the factor $\prod_{E+E'} Z_{xi}$. If this closed loop belongs to the homologically trivial class of the set of closed loops on the torus, we have

$$\prod_{E+E'} Z_{xi} = \prod_{P \text{ with in } E+E'} B_P = 1, \quad (13)$$

because of $Z_{xi}^2 = 1$ and the last equation of Eq.(6). Thus the correction is successful. On the other hand, if the closed loop belongs to the homologically nontrivial class, the first equality of (13) does not hold, hence the above correction procedure does not work.

Let us consider a toric code of an arbitrary large size and assume that the probability of error per qubit is p . An error chain E is characterized by a function of each link $n_E(\ell)$ ($\ell = \text{link}$) like $n_E(\ell) = 1$ for $\ell \in E$ and $n_E(\ell) = 0$ for $\ell \notin E$. As we explained above $E' = E + C$ where C is a cycle (i.e., a chain with no boundary) and then we define a function $n_C(\ell)$ for C in the exactly same way with $n_E(\ell)$. The probability that error chain E occurs is given as

$$\text{prob}(E) = \prod_{\ell} (1-p)^{1-n_E(\ell)} p^{n_E(\ell)}. \quad (14)$$

Let us consider the probability distribution for an arbitrary chain E' that has the same boundary with E , $\text{prob}(E'|E)^1$. For $\ell \in E'$ and $\ell \notin E$, the link functions are $n_C(\ell) = 1$ and $n_E(\ell) = 0$ and its probability is given as

$$\frac{p}{1-p}. \quad (15)$$

On the other hand for $\ell \notin E'$ and $\ell \in E$ with the link functions $n_C(\ell) = 1$ and $n_E(\ell) = 1$,

$$\frac{1-p}{p}. \quad (16)$$

¹The actual probability for the chain E' is given by $\text{prob}(E) \cdot \text{prob}(E'|E)$.

For $n_C(\ell) = 0$, the probability is unity. Then the conditional probability is given by (up to an irrelevant constant factor)

$$\text{prob}(E) \cdot \text{prob}(E'|E) = \prod_{\ell} \exp(J\eta_{\ell}u_{\ell}), \quad (17)$$

where

$$u_{\ell} = 1 - 2n_C(\ell) \in \{1, -1\}, \quad (18)$$

$$\eta_{\ell} = \begin{cases} 1, & \ell \notin E \\ -1, & \ell \in E, \end{cases} \quad (19)$$

and $e^{-2J} = p/(1-p)$.

From Eq.(18) and the fact that C is a close chain,

$$\prod_{\ell \in x} u_{\ell} = 1, \quad (20)$$

at each site x . The above constraint (20) can be easily solved by introducing classical Ising spin variables $\sigma_{x^*} = \pm 1$ at sites of the dual lattice,

$$u_{\ell} = \sigma_{x^*} \sigma_{x^*+i}, \quad (21)$$

where the notation is obvious. Then the generating function of the probability distribution of the error chains E' is given by the following partition function Z of the RBIM,

$$Z[J, \eta] = \sum_{\{\sigma_{x^*}\}} \exp\left(J \sum_{\ell} \eta_{\ell} \sigma_{x^*} \sigma_{x^*+i}\right). \quad (22)$$

The relation $e^{-2J} = p/(1-p)$ between the temperature and the concentration of the “wrong-sign” bonds p defines the Nishimori line[10]. (This condition of the Nishimori line will be explained in Sec.4.) It is straightforward to express each contribution to the above partition function Z pictorially in terms of the domain walls (see Fig.6). From the above discussion, it is obvious that if the RBIM is in the disordered phase, arbitrary large E' appears and successful error corrections are impossible. On the other hand, we can perform successful error corrections if the RBIM is in the ordered phase. The 2D RBIM has been studied well and its phase structure is known. When errors and noises throughout the measurement of the check operators are totally ignored, the accuracy threshold of the toric quantum memory is given by the intersection point of the phase boundary and the Nishimori line of the RBIM which is estimated as $p_c = 0.109$ [12].

Now let us proceed to the second step by taking into account the errors in measuring the check operators themselves. In this case, the error chains E live in the two-dimensional space and the one-dimensional time because we must repeat the check operations (syndrome measurements) many

times. Boundaries of the error chain E reside on sites of the original $3D$ lattice. In the $3D$ cubic lattice, a link of the original lattice corresponds to a plaquette of the dual lattice. Then the constraint (20) can be solved as

$$u_\ell = \prod_{P^*} \sigma_{\ell^*}, \quad (23)$$

where the plaquette P^* on the dual lattice corresponds to the link ℓ on the original lattice and σ_{ℓ^*} is the Ising variable on the link ℓ^* of the dual lattice. From Eqs.(17) and (23), the conditional probability $\text{prob}(E'|E)$ can be expressed as

$$\text{prob}(E) \cdot \text{prob}(E'|E) = \prod_{P^*} \exp(J\eta_{P^*} \prod_{\ell^* \in P^*} \sigma_{\ell^*}), \quad (24)$$

where $\eta_{P^*} = \eta_\ell = \pm 1$ and other notations are self-evident. Then the statistical-mechanical model in the present case is the RPGM defined on the $3D$ lattice. Its third direction represents the real time directions along which measurements are done, while each plane lying in the $1 - 2$ directions is the dual lattice of the original $2D$ lattice.

In the following section, we shall study the phase structure of the RPGM by numerical methods. Hereafter we assume that the error probability of syndrome measurement is also given by p for simplicity. We shall consider $3D$ lattice as large as possible. As discussed in Refs.[3, 4], the phase structure of an arbitrary large system gives the accuracy threshold of the toric code for the error correction.

4 Phase structure of the RPGM

In this section, we study the phase structure of the $3D$ Z_2 RPGM by MC simulations, and calculate the accuracy threshold for the toric quantum memory. The phase boundary is determined by calculating the specific heat and expectation values of the Wilson loop. We note that our choice of the above model implies that we take into account possible errors which may occur in the measurements of the check operators.

The partition function of the $3D$ RPGM is given by

$$Z(\beta, \eta) = \sum_{\{\sigma_{xi}=\pm 1\}} e^{-\beta E}, \quad E = - \sum_P \eta_P \prod_P \sigma, \quad (25)$$

where E is the energy and $\sigma_{xi} = \pm 1$ is a Z_2 classical variable sitting on the link (x, i) of the $3D$ dual lattice ($i = 1, 2, 3$).² $\prod_P \sigma$ denotes the product of four σ 's along the four links forming P . $\eta_P = \pm 1$

²As discussed in the previous sections, the present RPGM is defined on the *dual* lattice. In this section however, we shall use simple notations like P instead of P^* for the dual plaquette, etc.

is a *quenched* random variable on the plaquette P . The concentration of “wrong-sign” plaquettes with $\eta_P = -1$ is p as in the previous sections. Thus the weight function $P(K_P, \eta)$ for a set of η_P 's is given by

$$\begin{aligned} P(K_P, \eta) &= \prod_P [(1-p) \delta_{\eta_P, 1} + p \delta_{\eta_P, -1}] \\ &= (2 \cosh K_P)^{-N_P} \cdot \exp\left(K_P \sum_P \eta_P\right), \end{aligned} \quad (26)$$

where N_P is the total number of plaquettes, and the parameter K_P is related with p through the relations,

$$1-p \propto \exp(K_P), \quad p \propto \exp(-K_P), \quad \frac{1-p}{p} = e^{2K_P}. \quad (27)$$

Then the ensemble-averaged free energy $F(\beta, K_P)$ is defined as

$$F(\beta, K_P) = -\frac{1}{\beta} \sum_{\{\eta_P = \pm 1\}} P(K_P, \eta) \ln Z(\beta, \eta). \quad (28)$$

We presented in Fig.1 a schematic phase diagram of the RPGM in the $p-T$ plane. At $p = 0$, i.e., the Z_2 gauge system in 3D with a constant gauge coupling, it is known that there are two phases, one is the Higgs phase and the other is the confinement phase[9]. The critical coupling is estimated as $\beta_c = 0.76(T_c = 1.31)$. As the concentration p of “wrong-sign” plaquettes increases, the critical temperature $T_c(p)$ at p decreases and at a certain value of $p = p_0$, the critical temperature vanishes, $T_c = 0$. As discussed in the previous section, the system must be in the ordered Higgs phase for the toric code to work as a reliable quantum memory. In Fig.1 the Nishimori line $T = T_N(p)$ is plotted by the dashed line. In the high- T region *above* $T_N(p)$, the critical line is rather horizontal, whereas in the low- T region *below* $T_N(p)$, it is almost vertical.

The Nishimori line is defined in the $p-T$ plane by setting $K_P = \beta$, on which the quantum fluctuations of gauge field σ_{xi} and fluctuations caused by the “random impurity” η_P valance in magnitude, i.e., giving the same effect to disorder the system. Let us explain this briefly. For the case $p = 0$, there is no randomness, and the quantum(thermal) fluctuations are controlled by the Boltzmann factor $\exp(\beta \sum_P \prod \sigma)$. On the other hand at $T = 0$ with finite K_P , the quantum fluctuations are suppressed; σ_{xi} are frozen and synchronized as $\prod_P \sigma = \eta_P$ due to the factor $\exp(\beta \eta_P \prod_P \sigma)$ in Z . Thus the effects of randomness is controlled by the factor $P(K_P, \eta) \propto \exp(K_P \sum_P \prod \eta)$. These two factors become equal at $K_P = \beta$.

Let us choose the statistical-mechanical models as the method of error corrections in quantum computations. As discussed in Sec.3, we generate error-correcting chains E' exactly in the same way with error chains E , and this procedure corresponds to the Nishimori line in the $p-T$ plane. The critical line and the Nishimori line intersect with each other at $(p_c, T_N(p_c))$. In order that the toric

quantum codes to be fault-tolerant, the parameters of the toric codes, i.e., (p, T) , must be in the Higgs phase. The intersection point $(p_c, T_N(p_c))$ determines the maximum possible value of p for fault-tolerant codes, the accuracy threshold, as p_c .

Let us first focus on the high- T region. In Fig.7, we plot the specific heat per site, $c(\beta, p)$, as a function of T for various samples with $p = 0.005, 0.01, 0.015, 0.02$ and 0.025 . For $p = 0.005$ the peak of the specific heat develops as we increase the system size just as in the well studied case of $p = 0$. However, for $p = 0.01$, the peak does not develop as shown in Fig.8. For larger p 's, the peak of the specific heat disappears, although there seems to exist some discontinuities in the derivative $dc/d\beta$. Below we shall examine these anomalous behaviors of $c(\beta, p)$ by calculating the expectation values of the Wilson loops, and conclude that there certainly exist phase transitions at these values of p . The locations of these phase transitions are pointed with the arrows in Fig.7. The order of these transitions are weak second order or may be higher than 2. In Fig.9 we plot the critical temperature $T_c(p)$ of these phase transitions in the $p - T$ plane together with the solid Nishimori line. $T_c(p)$ starts from $T_c(0) = 1/0.76 = 1.31$ at $p = 0$ and decreases as p increases, as we expected.

To confirm the existence of the above phase transitions, we calculated the expectation values of the Wilson loop,

$$\begin{aligned} W(C) &= \sum_{\{\eta_P\}} P(K_P, \eta) \sum_{\{\sigma_{xi}\}} \left(\prod_C \sigma_{xi} \right) \frac{e^S}{Z(\beta, \eta)} \\ &= [W_{\text{sample}}(C)]_{\text{ens}}, \end{aligned} \quad (29)$$

$$W_{\text{sample}}(C) = \sum_{\{\sigma_{xi}\}} \left(\prod_C \sigma_{xi} \right) e^S / Z(\beta, \eta), \quad (30)$$

where C denotes a closed loop in the $3D$ lattice and $\prod_C \sigma_{xi}$ is the product of σ_{xi} 's along C . $W_{\text{sample}}(C)$ is the expectation value of the Wilson loop for *each sample* with fixed $\{\eta_P\}$ and $[\mathcal{O}]_{\text{ens}}$ denotes the ensemble average *over samples* of the quantity \mathcal{O} calculated for each sample. $W(C)$ is introduced by Wilson to characterize the confinement phase by the so called area law[9], that is, $W(C)$ behaves for large C 's as

$$W(C) \propto \exp(-\alpha A(C)), \quad (31)$$

where $A(C)$ is the smallest area of all the branes whose boundaries are C , and α is a constant called the string tension. On the other hand, in the deconfinement phase like the Higgs phase, $W(C)$ exhibits the following perimeter law for large C 's,

$$W(C) \propto \exp(-\gamma P(C)), \quad (32)$$

where $P(C)$ is the length of C . In Fig.10 $W(C)$ are plotted for $p = 0, 0.01$ and 0.02 from the above. We chose a pair of β 's for each p , slightly above and below $T_c(p)$ that are determined by

the calculation of the specific heat (see Fig.7). In the left column of Fig.10, $W(C)$ are plotted as $-\ln(W(C))/A(C)$ vs $A(C)$, so the curves become constant α when the area law (31) holds. In the right column of Fig.10, $W(C)$ are plotted as $-\ln(W(C))/P(C)$ vs $P(C)$, so the curves become constant γ when the perimeter law (32) holds. At all the pairs of β 's presented in the figures, we observe the changes in the behavior of $W(C)$ from the perimeter law at $T < T_c(p)$ to the area law at $T_c(p) < T$. These changes take place at temperatures very close to T_c , which confirm the existence of the phase transitions. The obtained value of $T_c(p)$ by the Wilson loop is *insensitive* to the distribution of the wrong-sign plaquettes, i.e., $\{\eta_P\}$ for fixed p .

Next we study the low- T region. We calculated the specific heat per site $c(\beta, p)$ along a line of fixed T by changing p , i.e., concentration of the wrong-sign plaquettes. For each p , we prepared 1000 samples, each of which has a definite configuration of $\{\eta_P\}$, and calculated the specific heat for each sample and averaged over the results. To obtain the suitable initial configuration of $\{\sigma_{xi}\}$ for each sample at low T , we employed the quenched-annealing method. In Fig.11, the averaged values of the specific heat for $\beta = 2.5$ are plotted from $p = 0.005$ to $p = 0.06$. We superimpose the fluctuations of each sample around the average. There exists a small discontinuity in $c(\beta = 2.5, p)$ at $p = 0.027 \sim 0.028$. As p increases, the fluctuations also reduce suddenly at $p = 0.027 \sim 0.028$ and they become almost constant for $p > 0.032 \sim 0.033$, so some kind of transition seems to occur there. As we show shortly, the same behavior of the specific heat is observed at $\beta = 2.0$. In order to verify the above expectation, we calculated the expectation values of the Wilson loop, $W(C)$ of (29). More precisely, we first calculated expectation value of the Wilson loop $W_{\text{sample}}(C)$ for each sample with *fixed* $\{\eta_P\}$. Typical results are shown in Fig.12 for $p = 0.013, 0.024, 0.025$ and 0.030 . It is obvious that a change of behavior of $W_{\text{sample}}(C)$ takes place from the perimeter law (32) to the area law (31) as p increases as we expected. In the region close to $p = 0.026$, some samples show the area law, whereas others exhibit the perimeter law. This result is in contrast to that of the high- T region.

In order to understand the implication of the above result, let us see the expectation value of the Wilson loop more precisely. From Eq.(29), it is obvious that the samples with the perimeter law dominate over those with the area law as $e^{-P(C)} \gg e^{-A(C)}$ for large C and $W(C)$ exhibits the *perimeter law* if samples with the perimeter and area laws *coexist*. We then examined $W_{\text{sample}}(C)$ for various but a finite number of samples by varying p and found that certain samples at $p = 0.025$ and 0.026 exhibit the perimeter law and others show the area law, i.e., the coexistence (we show the result of a sample with the area law for $p = 0.025$ in Fig.12). For larger values of p , we found only the area-law decaying $W_{\text{sample}}(C)$. (This does not mean that all samples exhibit the area law because we only examined a finite number of samples.) In this way we estimate a lower bound of the

critical value of p as $p \sim 0.026$, which is consistent with the calculations of the specific heat given in Fig.11.

We also studied the case of $\beta = 2.0$ which is close to the Nishimori line. In Fig.13, the specific heat and the fluctuations over samples are shown. On the Nishimori line, it is proved[10] that the specific heat exhibits *no* singular behaviors (no divergences). In fact, Fig.13 shows rather smooth behavior in $c(\beta, p)$. Let us examine the possibility of a phase transition by studying $W(C)$. In Fig.14 we present $W(C)$ at $\beta = 2.0$ for $p = 0.020, 0.030, 0.031$ and 0.040 . As p increases, we observe that the behavior of $W(C)$ changes from the perimeter to area law. As far as we observed, the maximum value of p at which $W(C)$ exhibits the perimeter law is 0.030 , and therefore we conclude that the phase transition from the Higgs phase to the confinement phase occurs near this value.

From the calculations of the specific heat and its fluctuations shown in Figs.11 and 13, we estimate the critical values of p as $p = 0.032 \sim 0.033$ at both $\beta = 2.5$ and $\beta = 2.0$. In both cases, the fluctuations of the specific heat become constant for $p > 0.032 \sim 0.033$. For the case of $\beta = 2.5$, if we regard the small discontinuity in the specific heat as the phase transition point, the critical value of p is estimated as ~ 0.027 . In order to obtain a definitive value of p_c , a thorough investigation on the Wilson loop is required.

5 Conclusion

In this paper, we studied the RPGM in 3D numerically and obtained the phase transition line in the $p - T$ plane which separates the Higgs and confinement phases. The critical concentration of the “wrong-sign” plaquettes is estimated as $p = 0.032 \sim 0.033$ at low T and also close to the Nishimori line. This result determines the accuracy threshold for the quantum toric code as $p_c \simeq 0.033$. In Ref.[4], the critical value of p along the $T = 0$ axis was estimated as 0.029 , which corresponds p_0 in Fig.1. This value gives a lower bound of p_c , and Fig.9 shows that our MC simulations are consistent with their calculations.

In Ref.[7] a qualitative phase diagram of the 3D Z_2 RPGM was obtained by using the replica methods, and the existence of the “gauge-glass phase” is predicted at relatively low T and moderate value of p . In the present calculations, however, there appears no sign of that phase. In the higher-dimensional gauge models, the gauge-glass phase may exist.

It was recently suggested that anyonic excitations in Kitaev’s model with discrete non-Abelian gauge groups may play an important role in constructing quantum gates of QC’s[5, 6]. Then generalization of the present study of the Z_2 model to a non-Abelian gauge model is interesting.

References

- [1] A.Yu.Kitaev, “Quantum error correction with imperfect gates”, in *Proceedings of the Third International Conference on Quantum Communication and Measurement*, ed. O.Hirota, A.S. Holevo, and C.M. Caves (New York, Plenum, 1997); “Fault-tolerant quantum computation by anyons”, quant-ph/9707021; *Annals Phys.*303, 2(2003); M.Freedman, A.Kitaev, M.Larsen, and Z.Wang, “Topological quantum computation”, quant-ph/0101025.
- [2] J.Preskill, “Fault-tolerant quantum computation”, quant-ph/9712048;
- [3] E.Dennis, A.Kitaev, A.Landahl, and J.Preskill, “Topological quantum memory”, quant-ph/0110143; *J.Math.Phys.*43, 4452 (2002).
- [4] C.Wang, J.Harrington and J.Preskill, “Confinement-Higgs transition in a disordered gauge theory and the accuracy threshold for quantum memory”, quant-ph/0207088; *Annals Phys.*303, 31 (2003).
- [5] C.Mochon, *Phys.Rev.A*67, 022315(2003).
- [6] B.Douçot, L.B.Ioffe, and J.Vidal, “Discrete non-Abelian gauge theories in two-dimensional lattices and their realizations in Josephson-junction array”, cond-mat/0302104.
- [7] G.Arakawa and I.Ichinose, “ Z_N gauge theory on a lattice and quantum memory”, quant-ph/0309142; *Annals Phys.*311, 152(2004).
- [8] K.Takeda and H.Nishimori, “Self-dual random-plaquette gauge model and the quantum toric code”, hep-th/0310279; *Nucl.Phys.B* (in press).
- [9] See for example, J.Kogut, *Rev.Mod.Phys.*51, 659(1979).
- [10] See Ref.[4] and references cited therein; H.Nishimori, “*Statistical Physics of Spin Glasses and Information Processing*” (Oxford University Press, 2001).
- [11] E.Knill, R.Laflamme and W.H.Zurek, *Proc.Roy.Soc.Lond. A* 454, 365(1998); D.Aharonov and M.Ben-Or, “Fault-tolerant quantum computation with constant error”, quant-ph/9611025; “Fault-tolerant quantum computation with constant error rate”, quant-ph/9906129; A.Yu.Kitaev, *Russian Math.Surveys* 52, 1191 (1997); J.Preskill, *Proc.Roy.Soc.Lond. A* 454, 385(1998); D.Gottesman, “Stabilizer codes and quantum error correction”, quant-ph/9705052.
- [12] See Ref.[4] and references cited therein.

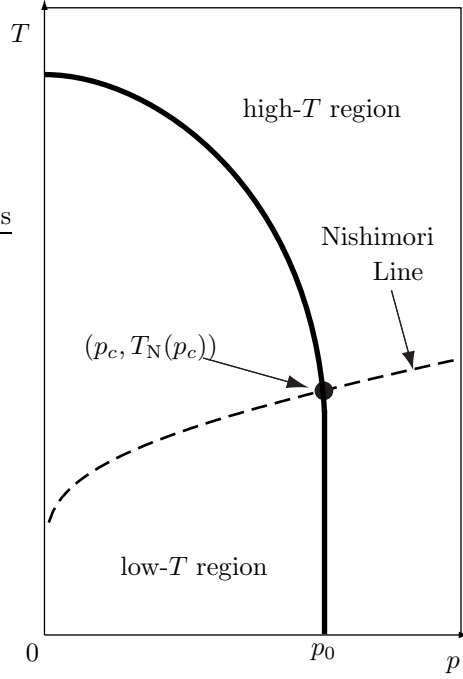


Figure 1: A schematic phase diagram of the $3D Z_2$ RPGM in the $p - T$ plane, where p is the concentration of wrong-sign plaquettes and $T = \beta^{-1}$ is the “temperature” (the gauge coupling constant). The thick curve is the phase-transition line $T_c(p)$ which separates the ordered Higgs phase and the disordered confinement phase. The dashed line $T_N(p)$ is the Nishimori line which corresponds to the present methods of the error corrections in quantum computations. The value p_c at the intersection point $(p_c, T_N(p_c))$ determines the accuracy threshold for the quantum toric code.



Figure 2: The original lattice (a) with periodic boundary condition and its dual lattice (b). C_Z^1, C_Z^2 , are two noncontractible closed loops on (a) in the horizontal and vertical directions, while $\tilde{C}_X^1, \tilde{C}_X^2$ are corresponding loops on the dual site.

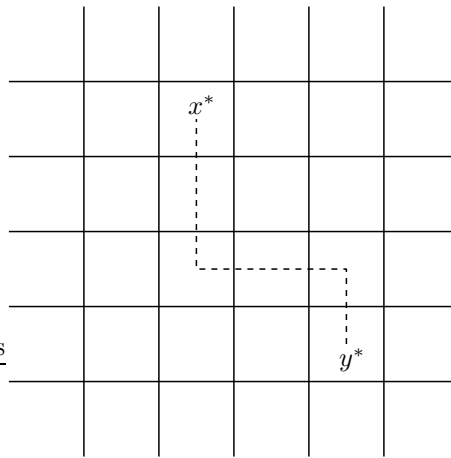


Figure 3: Path $\tilde{C}_{x^*y^*}$ connecting dual sites x^* and y^* .

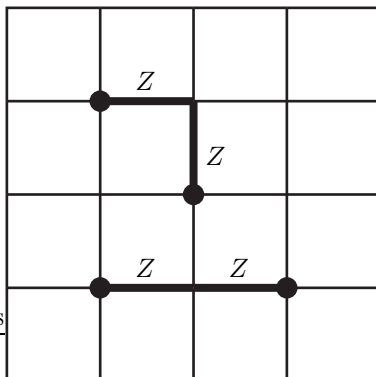


Figure 4: Typical example of error syndrome produced by noises. The error sites are marked by filled circles, where the check operators are $A_x = -1$. They are connected by the error links marked by thick links, on which extra Z_{x_i} 's are applied.

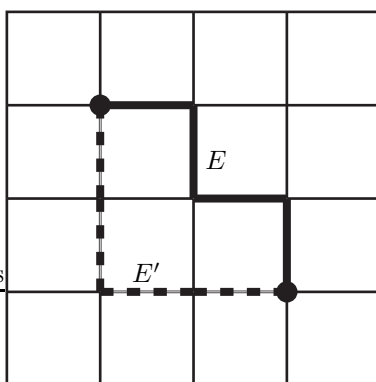


Figure 5: An error chain E produced by noises and an applied chain E' produced in the process of the error correction. Both E and E' connect the pair of error sites and $E + E'$ form a closed loop, i.e., a cycle.

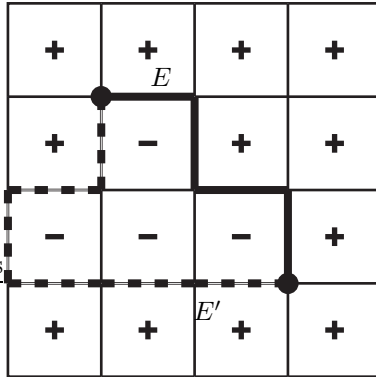


Figure 6: Domain wall is produced along the cycle of the error chain E and the error-correction chain E' . Corresponding configuration in the partition function (22) is achieved by the configuration of the dual variables, $\sigma_{x^*} = -1$ within the wall and $\sigma_{x^*} = +1$ outside the wall.

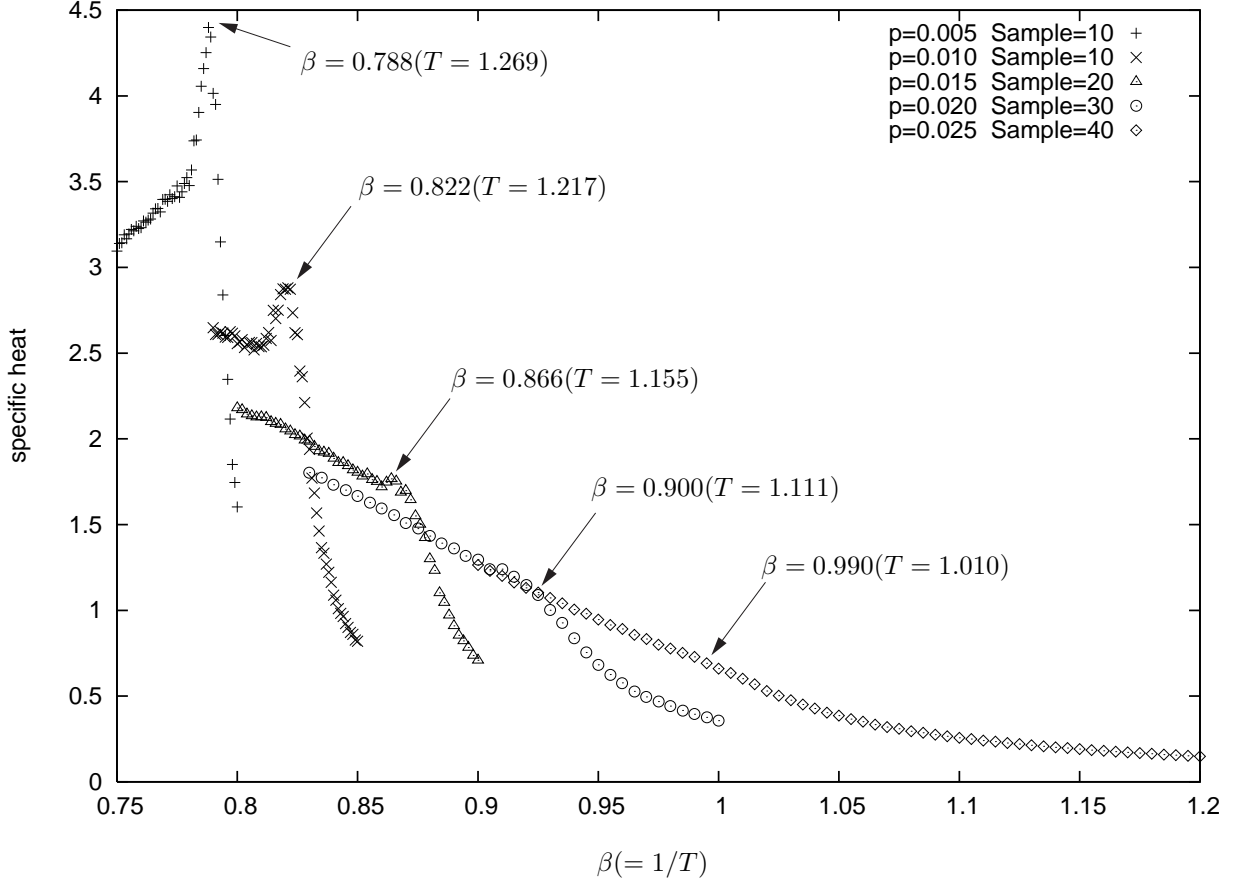


Figure 7: Specific heat per site in the high- T region vs β . In the MC simulation, the size of the $3D$ lattice is $N_v = 24^3$ sites, and the numbers of sweeps are 20000 for thermalization and 100000 for measurement for $p=0.005, 0.010$ and 0.015 , and 30000+100000 for $p=0.020$ and 0.025 . We averaged over 10 ~ 40 samples with different configurations of η_P . The positions marked by arrows denote the locations of phase transitions confirmed by measuring the Wilson loops.

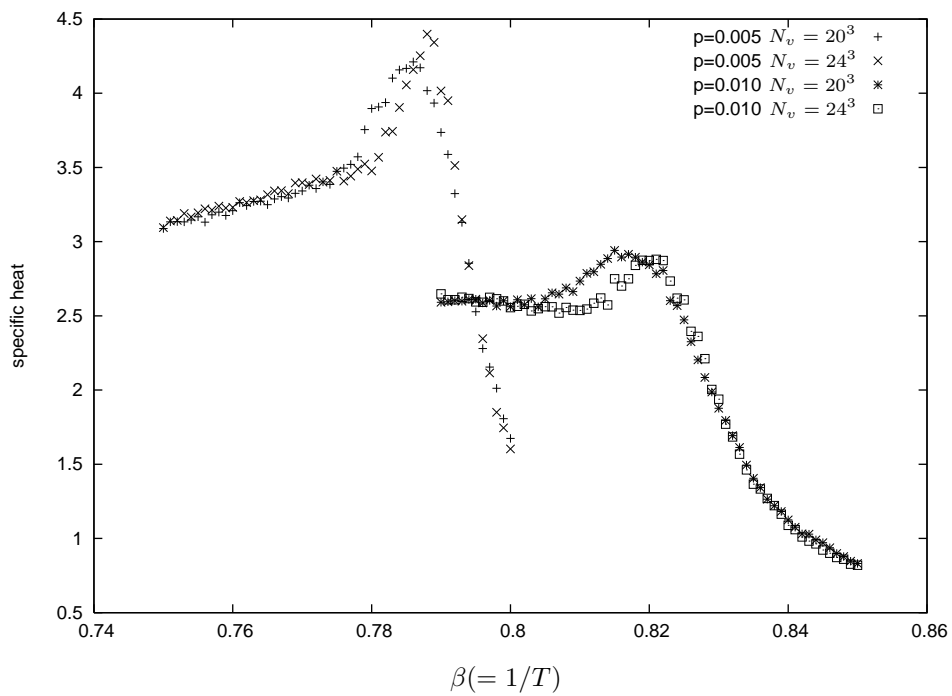


Figure 8: Specific heat vs β for $p = 0.005, 0.01$. For $p = 0.005$, the peak develops as the system size increases, exhibiting a second-order transition. For $p = 0.01$, the size dependence is very weak and the order of the transition seems to be very weak second order or higher than second-order.

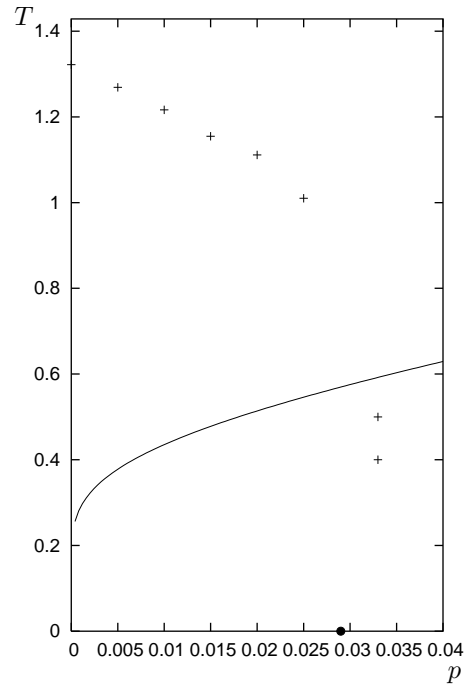


Figure 9: Phase diagram in the $p - T$ plane. The crosses denote the phase transition points $T_c(p)$ determined by the specific heat and the Wilson loops. The solid line is the Nishimori line $T_N(p)$. As T is lowered, the critical value of p starts to increase, and then decreases. This bending behavior of $T_c(p)$ makes the problem of finding the best method of error corrections nontrivial. The statistical-mechanical methods of the error correction discussed in Sec.3 correspond to the Nishimori line, which gives a higher accuracy threshold $p_c \simeq 0.033$ than $p_0 = 0.029$ determined by $T_c(p_0) = 0$ [4].

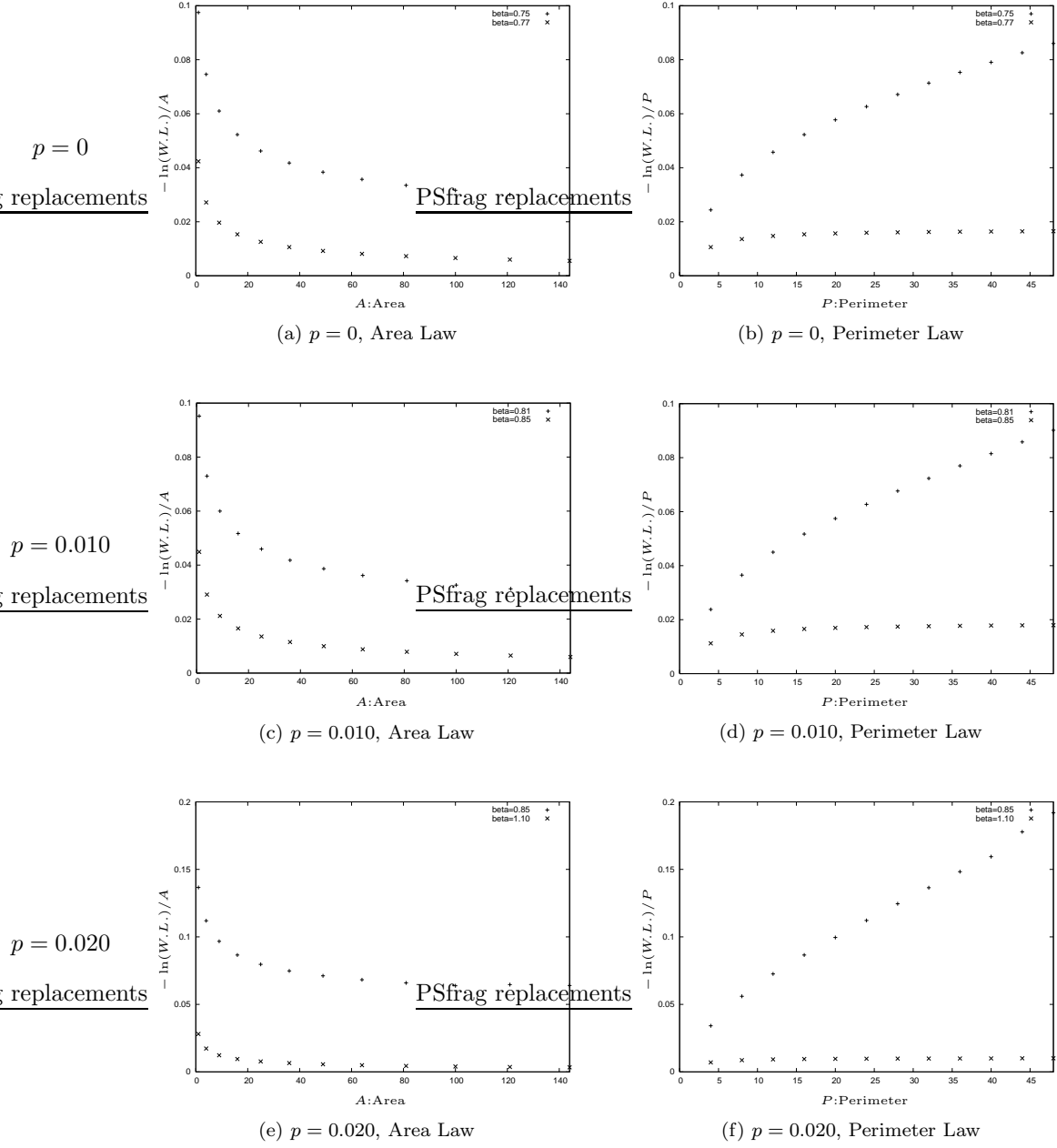


Figure 10: Wilson loops $W(C)$ in high- T region. The size of the lattice is $N_v = 24^3$. The results are plotted in the pair of axes, $A(C)$ (the smallest number of the plaquettes in all the branes bounded by the loop C) and $-\ln(W(C))/A(C)$ in the left column, and $P(C)$ (the number of links contained in C) and $-\ln(W(C))/P(C)$ in the right column. If the area(perimeter) law (31)((32)) holds, the curves in the left(right) column become constants $\alpha(\gamma)$.

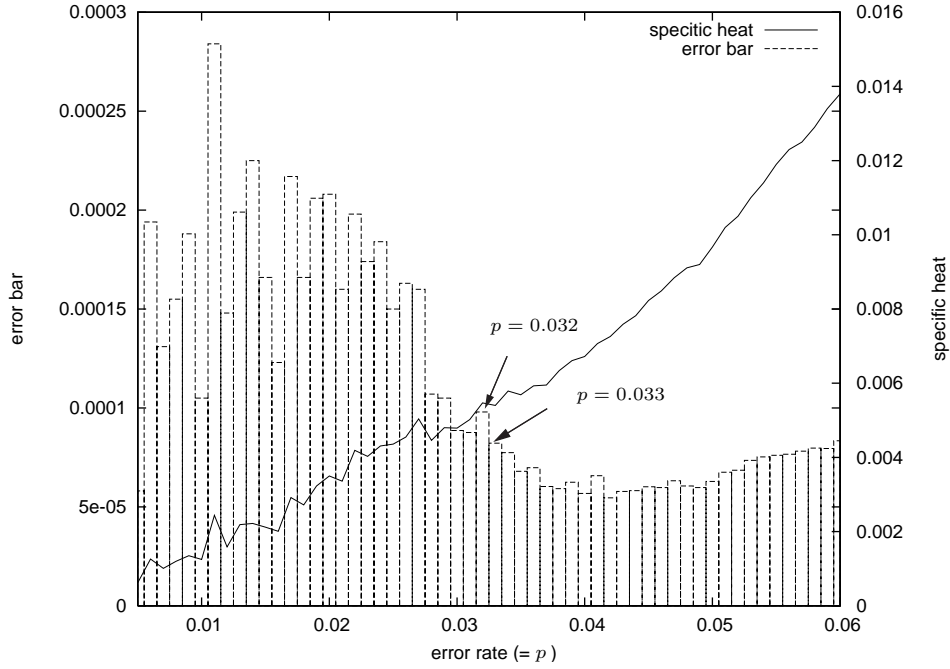


Figure 11: Specific heat in the low- T region at $\beta = 2.5$ vs p . The histogram denotes the fluctuations at each p over 1000 samples around the average. As p increases, the fluctuation decreases and suddenly reduces to an almost constant value at $p \simeq 0.033$ marked by arrows. This value almost coincides with the critical value determined by $W(C)$ in Fig.12.

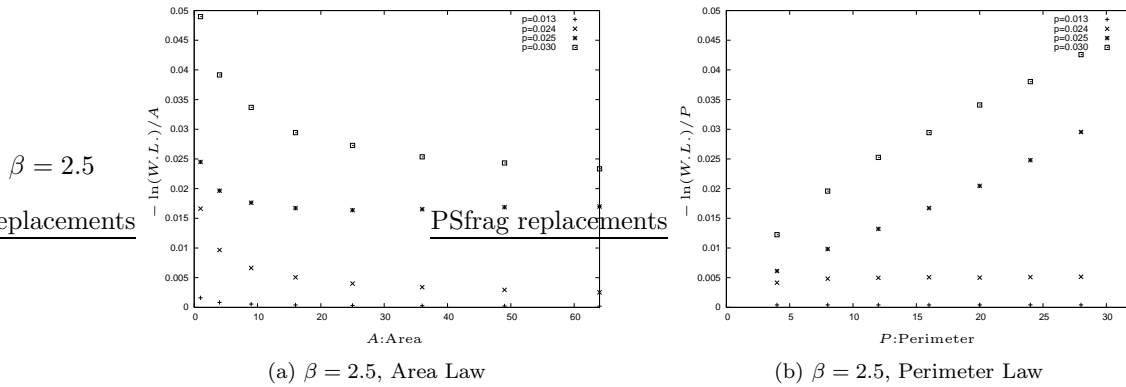


Figure 12: Wilson loop $W_{\text{sample}}(C)$ for certain samples in the low- T region at $\beta = 2.5$. The size of the lattice is $N_v = 16^3$. At $p = 0.025$ it exhibits the area law, while at $p = 0.024$, the perimeter law. This result gives a lower-bound estimate of the value of p on criticality, which is consistent with the specific-heat calculations in Fig.11. (See text.)

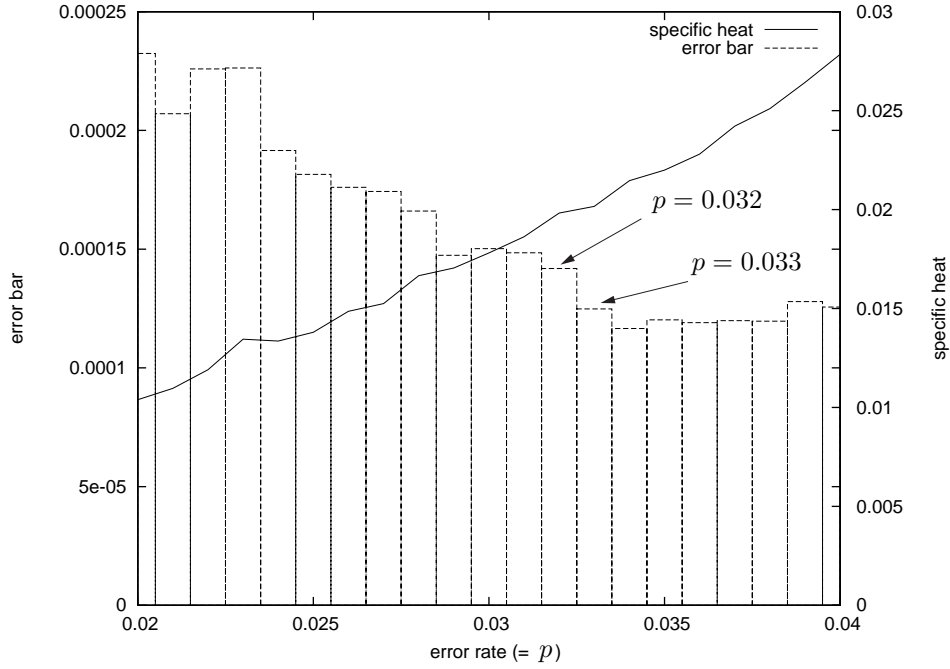


Figure 13: Specific heat and fluctuations at $\beta = 2.0$. Similar plot as in Fig.11. As p increases, the fluctuation reduces gradually, and reaches at a constant value at $p \simeq 0.033$ as marked with arrows. This value almost coincides with the critical value studied by the Wilson loops in Fig.14.

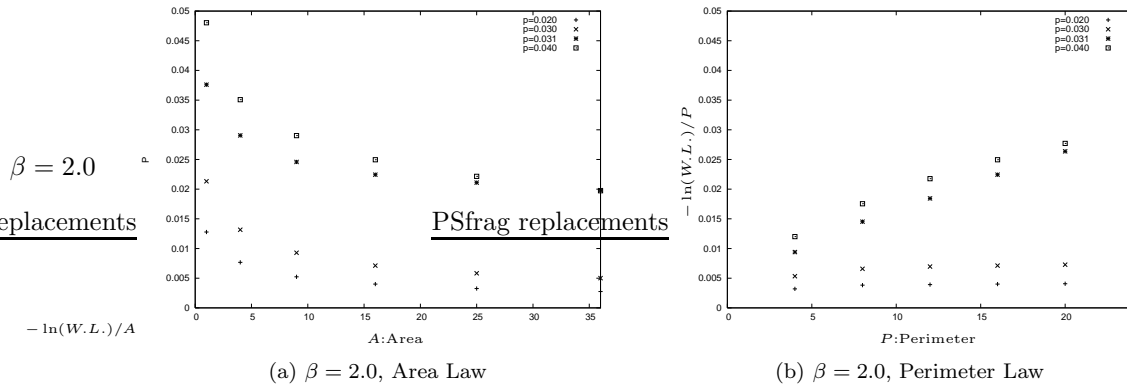


Figure 14: Wilson loop in the low- T region at $\beta = 2.0$. The size of the lattice is $N_v = 12^3$. Similar plot as in Fig.12. We observe that the change in the behavior of $W(C)$ from the area law to the perimeter law takes place at $p \simeq 0.031$. This critical value almost coincides with $p \simeq 0.033$ discussed in Fig.13.